Available online at www.CivileJournal.org

Civil Engineering Journal

(E-ISSN: 2476-3055; ISSN: 2676-6957)

Vol. 8, No. 07, July, 2022

Numerical Analysis of Seepage Failure Modes of Sandy Soils within a Cylindrical Cofferdam

Aissa Bensmaine [1*], Naïma Benmebarek [1], Sadok Benmebarek [1]

[1] *Department of Civil and Hydraulic Engineering, NMISSI Laboratory, Biskra University, BP 145 Biskra 07000, Algeria.*

Received 19 April 2022; Revised 16 June 2022; Accepted 23 June 2022; Published 01 July 2022

Abstract

Soil seepage failure within cofferdams is a dangerous phenomenon that always poses difficulties for designers and builders of excavations in zones with high water levels. When the hydraulic head difference H between the upstream and downstream sides reaches a critical height, the downstream soil seepage failure occurs. Depending on soil properties, soil-wall interface characteristics, and cofferdam design, different seepage failure modes can be observed: heaving, boiling, liquefaction, or failure by reduction of the passive earth pressure. In the literature, there are differences, sometimes very large, in the critical value of the hydraulic head loss H_c/D inducing seepage failure given by several methods proposed for stability verification. Then, complex cases are generally approached using simplifying assumptions and adopting large safety factors to take account of uncertainties. In practice, geotechnical engineers deal with many kinds of excavations and different shapes of cofferdams, such as rectangular, square, or circular, which generate three-dimensional (3D) flow conditions. Axisymmetric seepage flow through the soil in a circular cofferdam is often used to model such 3D seepage flow. In this paper, using the numerical code FLAC, several numerical simulations are carried out in axisymmetric groundwater flow conditions to analyze the seepage failure modes of cohesionless sandy soils within a cylindrical cofferdam. The effects of the cofferdam radius, internal soil friction, soil dilatancy, and interface friction on the H_c/D value and failure mode are studied. The numerically obtained seepage failure modes are presented and discussed in various scenarios. The present results, illustrated in both tables and graphs, show a significant decrease in the value of H_c/D inducing seepage failure, with a decrease in the cofferdam radius. They also indicate the sensitivity of the seepage failure mode to internal soil friction, soil dilatancy, interface friction, and cofferdam radius. As well, new terms are proposed for the seepage failure mode designations based on the 3D view of the downstream soil deformation.

Keywords: GNSS Network; Excavation within Cofferdams; Seepage Failure; Critical Hydraulic Head Loss; Sandy Cofferdam Failure.

1. Introduction

The construction of infrastructure, such as bridge pillar foundations, deep basements, and underground transportation systems, often requires deep excavations within cofferdams. These are often used to stabilize excavations and keep them out of water to secure the site during construction. The cofferdam design at high water levels is often dominated by the seepage of water through soil around the sheet pile wall. The upward seepage flow, induced by the water level lowering (excavation dewatering), influences the cofferdam wall and the excavation base stabilities where seepage failure by bulk heaving, boiling, liquefaction or failure by reduction of the passive earth pressure may occur. There are many published methods for the assessment of excavation bottom stability against seepage failure, but sometimes failures occur even in deep excavations within cofferdams designed by these methods [1, 2]. There are several situations that cannot be predicted by conventional soil column approaches or the two-dimensional (2D) seepage flow model. Many sorts of

* Corresponding author: aissa.bensmaine@univ-biskra.dz

http://dx.doi.org/10.28991/CEJ-2022-08-07-06

excavation are encountered using single sheet pile walls, causing two-dimensional flow (2Dflow) conditions, or double sheet pile walls, generating 2D concentrated flow (2DCflow), or various cofferdam shapes in a plan view, rectangular, square, or circular, engendering three-dimensional flow (3Dflow) conditions. An axisymmetric seepage flow through soil within a circular cofferdam is often used to model such a 3D seepage flow. The circular cofferdam induces the axisymmetric flow (AXSflow) conditions. The 3D effect of water flow around cofferdams increases the water pressure to make failure occur easily [3]. Compared to 2DCflow conditions (double sheet pile walls case), the concentration of seepage flow into soil within circular cofferdam in AXSflow conditions is strongly accentuated and the safety factor against seepage failure of soil surrounded by the circular wall is lower. And, from the point of view of the critical hydraulic head difference H_c, it is not reasonable from the point of view of the 2DCflow as 2Dflow and to assume the AXSflow as 2DC-or 2Dflow [4, 5]. The risk assessment of soil seepage failure behind sheet piles has been studied and discussed by many researchers. Therefore, several methods, theories, and discussions were respectively proposed and recorded in the literature.

Terzaghi's method [6] based on reduced physical model experiments using one-layered sand. The sheet pile is fixed and embedded at a depth D below the horizontal surface level of the subsoil which has a thickness T as shown in Figure 1. The hydraulic head difference H between up- and downstream side induces seepage flow through sand. The sand deformations occur by steps with increasing H. The sand adjacent to the sheet pile remains stable as long as H is below a certain critical value. However, when this critical value is reached, the downstream sand surface heaves and the subsoil collapses. The most dangerous upheaved zone observed is confined to a body of sand adjoining the sheet pile. The sand body heaved by the upward seepage flow is assumed by Terzaghi [6], from experimental evidence, having a rectangular prism shape with width equal to $D/2$ and a horizontal base located at some depth D_0 below the surface ($0 \leqslant D_0 \leqslant D$). The heaving of sand prism $OABC$ is resisted by the weight and the vertical side shearing resistance such as friction and cohesion of soil prism. At the instant of seepage failure, it is assumed that the effective horizontal stress on the sand prism sides OC and AB, and the corresponding frictional resistance are practically zero. For sand, the cohesion is also practically zero. Then, as soon as the resultant force of the excess pore water pressure U_e on the sand prism base OA becomes equal to the sand prism submerged weight W', the prism upheaves.

$$W' = \frac{D}{2} D_0 \gamma' \tag{1}$$

$$U_e = \frac{1}{2} D_0 \gamma_w D h_a = \frac{1}{2} \gamma_w D C_0 H \tag{2}$$

where γ' is the buoyant unit weight of soil, γ_w is the unit weight of water, ha (= C_0H) is the average excess hydraulic head, and C_0 is a constant, assumed to be independent of H. The hydraulic head difference at the instant of the sand prism heaving H_0 is calculated from Equations 1 and 2 as follows:

$$W' = U_e \Rightarrow H_0 = \frac{D_0 \gamma'}{C_0 \gamma_w} \tag{3}$$

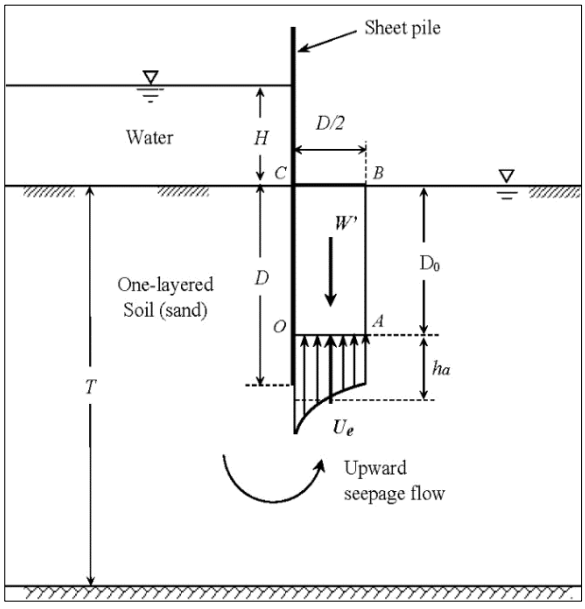

Figure 1. Seepage failure by heaving (Terzaghi's method, 1943)

The calculation is repeated for different horizontal section, through the sand, located at different depths D_0 below the bottom of the pit. The critical head difference H_c is determined by the condition H_0 = minimum:

$$H_c = \min\left\{H_0 = \frac{D_0\gamma'}{C_0\gamma_w}\,;0 \le D_0 \le D\right\} \quad \text{(By Terzaghi, 1943 [6])} \tag{4}$$

The horizontal section to which this minimum refers is the critical section. On the other hand, in Terzaghi & Peck method [7], for the one-layered sand shown in Figure 1, the special case of $D_0 = D$ is considered because they found that the critical section passes almost exactly through the lower edge of the wall ($D_0 = D$). The critical hydraulic head difference H_c then is given by:

$$H_c = \frac{D_0\gamma'}{C_0\gamma_w} = \frac{D\gamma'}{C_0\gamma_w} \quad \text{(Terzaghi \& Peck, 1948 [7])} \tag{5}$$

At a given value of hydraulic head difference H, the safety factor against seepage failure of a sand prism F_s is given as a ratio of W' to U_e, from Equations 1, 2 and 3:

$$F_s = \frac{W'}{U_e} = \frac{DD_0\gamma'/2}{h_aD\gamma_w/2} = \frac{D_0\gamma'}{C_0\gamma_w}\,\frac{1}{H} = \frac{H_0}{H} \tag{6}$$

F_s can also be expressed by:

$$F_s = \frac{W'}{U_e} = \frac{D_0\gamma'}{C_0\gamma_w}\,\frac{1}{H} = \frac{D_0 i_c}{C_0 H} = \frac{i_c}{i_m} \tag{7}$$

where i_m is the average hydraulic gradient between *OA* and *CB* (Figure 1), and i_c is the critical hydraulic gradient.

$$i_m = \frac{C_0 H}{D_0} = \frac{h_a}{D_0} \tag{8}$$

$$i_c = \frac{\gamma'}{\gamma_w} = \frac{G_s - 1}{1+e} \tag{9}$$

where G_s is the specific gravity of solid soil particles, and e is the void ratio of soil. The safety factor against seepage failure of the soil behind the sheet piles $F_{s\,min}$ is determined by the condition F_s equal to minimum:

$$F_s = min\left\{F_s = \frac{W'}{U_e} = \frac{i_c}{i_m} = \frac{H_0}{H}\;;\; 0 \le D_0 \le D\right\} \tag{10}$$

And, from Equations 4 and 10, F_s is given by:

$$F_s = \frac{H_c}{H} \tag{11}$$

Terzaghi's method [6] initiated the prismatic failure concept and defined the critical hydraulic gradient criterion which controls the phenomenon of piping or boiling on one-layered homogeneous sand in 2Dflow conditions. It should be noted that, Terzaghi's method [6, 7] was formulated for 2D problem and may not be applied to estimate a safety factor against seepage failure in AXSflow conditions [4].

McNamee [8] registered two main forms of seepage failure relating to sheet piles wall: local failure in the form of "piping" or "boiling" and general "heaving'' and formulated a safety factor F_s against seepage failure by boiling as equal to the ratio of the critical gradient i_c to the exit gradient i_e at the excavation level, hence:

$$F_s = \frac{i_c}{i_e} \tag{12}$$

Marsland [9] carried out extensive tests on a reduced physical model using homogeneous sand in an open water excavation, by testing two types of sand, loose and dense sand. In loose sand, he noted that seepage failure occurs in downstream sand when the pressure at the bottom tip of the sheet pile wall is sufficient to uplift the submerged sand column adjoining the sheet pile (the width equal to *D/2* is not mentioned). And that seepage failure occurs when the exit gradient at the excavation bottom surface reaches a critical value in dense sand case. By comparing the effective soil weight and the water seepage pressure, Davidenkoff [10] showed that massive uplift of soil rectangular prism is only possible if the vertical shear forces on the prism sides are neglected and its width is less than that mentioned by Terzaghi's method. The author concluded that soil prism seepage failure starts from the sheet piles bottom tip for homogeneous soils, hence:

$$F_s = \frac{i_c}{i_m} \tag{13}$$

Davidenkoff and Franke [11] proposed a diagram based on a studied model, which can be used to determine the safety factor against seepage failure by piping for excavations in open water with different thickness of the pervious stratum. It should be noted that for the case of a sheet piles wall embedded in homogeneous and isotropic semi-infinite

soil, the differences recorded between the safety factors against seepage failure resulting from these various approaches are very considerable and reach up to 75% as reported by Kastner [12].

Tanaka & Verruijt [13] analysed experimentally and numerically, the seepage failure phenomenon of one-layered isotropic sand behind sheet piles, by using respectively a test apparatus and a numerical finite elements method (FEM) analysis in 2Dflow conditions. Through their experiments, they observed precisely the seepage failure mechanism. They proposed a practical approach to analyses this phenomenon by analytically developing a prismatic failure concept in both cases no-friction and friction on prism sides at the instant of failure. A safety factor has been formulated for each case. This concept is an extension of Terzaghi's method and is considering various prisms of smaller and larger widths. The critical prism is determined by the condition that the minimum safety factor among all of prisms becomes just equal to one, which is detected through the numerical representation of the equi-safety-factor lines. Their numerical results revealed that for prismatic failure (No-friction case), the critical prisms have zero width. And for prismatic failure (Friction case), the critical prisms have a width smaller than that of Terzaghi's method in which the width is fixed equal to *D/2*.

Using the variational approach applied to limit equilibrium method, Soubra et al. [14] published the passive earth pressure coefficients results in the presence of hydraulic gradients. Their results showed that passive earth pressure vanishes completely at the same value of hydraulic head loss $H/D = 2.78$ for different soil and interface friction angles. They concluded that soil and soil-wall interface characteristics have no effect on the H_c/D value causing seepage failure by heaving. For the same case, Terzaghi's approach gives a hydraulic head loss value against seepage failure by heaving equal to $H_c/D = 2.82$, while the seepage failure by boiling phenomenon occurs with a theoretical hydraulic head loss value equal to $H_c/D = 3.14 = \pi$. This phenomenon appears for a critical hydraulic gradient at the base of sheet pile wall point *C* (Figure 1). Benmebarek et al. [15] performed numerical simulations (FLAC code) in 2Dflow conditions and identified the different seepage failure modes occurring by boiling or heaving behind sheet piles wall. Their results indicated that the H_c/D value increases with the increase in internal soil friction angle φ, interface soil-wall friction δ and soil dilatancy angle ψ. For large friction angle φ, the H_c/D value was found in good agreement with theoretical value and the seepage failure mechanism mode is significantly influenced by the soil dilatancy angle. Then, by varying the ratio of horizontal to vertical soil permeability k_h/k_v, Benmebarek et al. [16] studied the permeability anisotropy effect on H_c/D causing soil seepage failure within cofferdam embedded in homogeneous horizontal sandy soil. Their results have shown that the increase in the permeability anisotropy k_h/k_v increases the seepage failure zone width and decreases the H_c/D sensitivity to the soil and interface characteristics.

Using the conventional flow net method and numerical analysis, Pratama & Ou [17] carried out a parametric studies series to clarify the safety factor values representing the safety against sand failure by boiling and to predict the seepage failure mechanism. The results showed that the critical soil prism width is smaller than that postulated by Terzaghi's method as pointed out by Benmebarek et al. [15]. A computational fluid dynamics solver involving two fluid phases and coupled with discrete element method software was developed by Xiao & Wang [18] to simulate the piping process around a sheet pile/cut-off wall. Their results indicate that heave behaviour occurs when the drag force located adjacent to the boundary on the downstream side is larger than the corresponding weight of the bulk soil. Then, using the same approach as that of the Xiao & Wang [18], Xiao [19] simulated the seepage failure process for the three phases of soil, water and air. The soil specimens used were made with two layers of graded particles to give different permeability properties in the vertical direction. They observed more heaving-type failure for the sample with higher permeability in the upper layer. The results indicate that the air bubbles impact would accelerate the development of heaving or boiling phenomenon and influence the system stability at an early stage.

Benseghier et al. [20] proposed a parallel computation framework of the lattice Boltzmann (LB) method and the discrete element (DE) method using a graphics processing unit and showed its application to geotechnical and erosion problems. Using microscale-coupled methods, Fukomoto et al. [21] present an application of a 2D coupled fluid-particle simulation model with no macroscopic assumptions to the seepage failure of saturated granular soils. Their used approach consists in coupling the LB method and the DE method to directly solve the seepage flow and the soil particles motion. Their results showed that a typical behaviour series for seepage failure can be seamlessly reproduced, where boiling and heaving initially occur on the downstream side near the sheet pile and finally lead to quicksand.

However, there is very little literature available on the resolution methods for seepage flow problems in 3Dflow conditions relating to square, rectangular or circular cofferdams. Few studies have presented design charts using numerical simulations in 3D- or AXSflow conditions for circular cofferdams [22-24].

To analyse the soil seepage failure within a circular cofferdam, Tanaka et al. [4] have developed an extension of prismatic failure concept, presented by Tanaka & Verruijt (1999) [13] and Tanaka et al. [25, 26], to the AXSflow condition. They assumed that the soil body upheaved by the upward seepage flow has a ring shape with a certain height and width adjoining the circular wall, and they considered the case where the side frictional resistance is not zero at the

instant of failure as shown in Figure 2. The frictions F_L et F_R on the left and right prism sides are exerted due to the presence of the horizontal effective stress σ'_x (Figure 2). The heave of the prism *OABC* is resisted by the submerged weight *W'* and the side frictions F_L and F_R. The safety factor against heaving of the soil prism *OABC*, which is submerged at the total water excess pressure on its base U_e, is given by:

$$F_s = \frac{W' + F_L + F_L}{U_e} \tag{14}$$

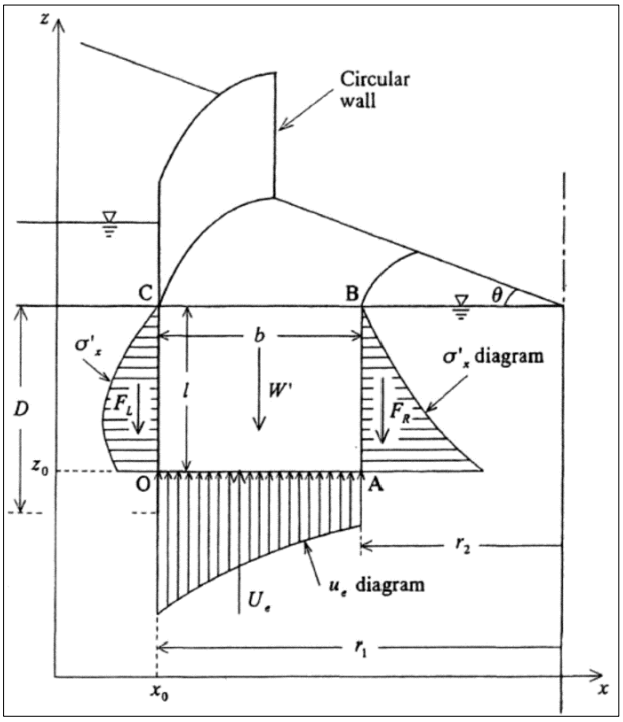

Figure 2. Prismatic failure considering friction in AXISflow conditions [4]

The critical prism is determined by the condition that the minimum safety factor $F_{s\,min}$ among all of prisms becomes just equal to 1.0. From failure experiments in AXISflow conditions, the authors [4] have discussed the sand seepage failure types. When *H* increases and approaches the hydraulic head difference at failure H_f, the upstream soil surface subsides and the downstream one heaves. The upstream subsidence has a ring-shaped wedge adjoining the wall (Figure 3). But, the change in the downstream soil surface configuration depends on the ratio (*D/R*) of the wall penetration depth *D* to the circular cofferdam radius *R* (Figure 3). For a small value of *D/R*, they observed a soil bulk having a certain width (Figure 3-a). On the other hand, for a large value of *D/R*, the whole soil upheaves (Figure 3-b), and after a few seconds the downstream soil is spouted out in the water. According to the surface deformation of downstream soil, the soil failure type is termed by the authors [4] as "Ring-type failure" for the small value of *D/R* and "Punching failure" for a large value of *D/R*. They considered three radius values *R* = 3, 5 and 10 m. For *R* = 3 and 5 m, depending on the value *D/R*, Ring-type failure and Punching failure occur. But for *R* = 10 m, independent of the value *D/R*, only the Ring-type failure occurs when *H* increases beyond H_c.

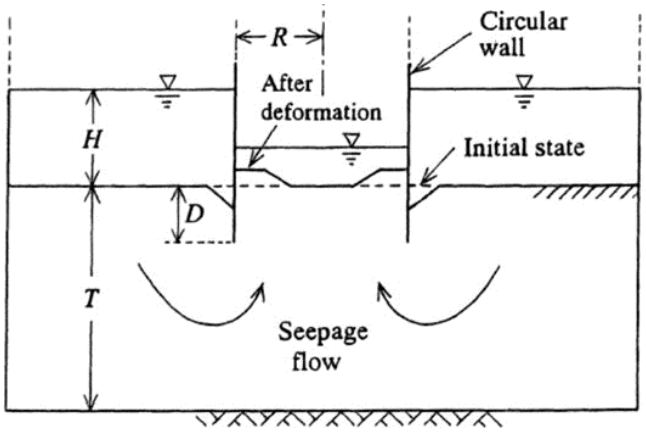

(a) Ring-type failure when *D/R* is small (or when *R/D* is large)

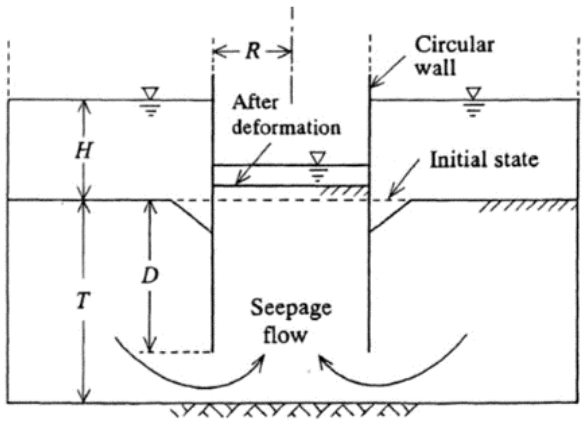

(b) Punching-type failure when *D/R* is large (or when *R/D* is small)

Figure 3. Seepage failure types in AXISflow conditions [4]

Employing the coupled LB method and the DE method, Fukumoto & Ohtsuka [27] examined the seepage failure induced by an upward seepage flow in 3Dflow conditions. Based on the experimental tests in 2Dflow conditions and the numerical simulations in 2D- and AXISflow conditions, Koltuk et al. [28] examined the seepage failure due to heaving in sheeted excavation pits in stratified cohesionless soils where a relatively permeable soil layer lies above a less permeable one between the excavation base and the wall tip. Their researches have revealed that such continuum approaches are an effective numerical tools against seepage failure around sheet piles.

Madanayaka et al. [29] presented simple solutions for estimating the flow rates and exit hydraulic gradients of square and rectangular cofferdams, they also compared the obtained solutions with those provided in the Canadian Foundation Engineering Manual (CFEM) in 2006 [30]. Then, by comparing with numerical and experimental models, Madanayaka and Sivakugan [31] validated the fragment method to estimate the hydraulic exit gradient and the flow for circular cofferdams in AXSflow conditions.

Zhao et al. [32] conducted both numerical analysis (FEM) and full-scale field tests on shaft construction project located in Guangzhou (China), to examine the circular shaft diameter effects on seepage failure by heaving and to analyse its failure mechanisms, as well as to develop a reasonable method of evaluating the stability of the circular shaft exposed to hydraulic upheave. The authors found that the results obtained from the FEM analysis are in good agreement with the phenomena observed at the site.

By using the numerical FEM PLAXIS code in AXISflow conditions, Ouzaid et al. [33] investigated the stability against seepage failure of a real deep excavation project in a circular cofferdam located in Ruhrgebiet (Germany), subjected to seepage flow. Then, a vertical drainage system formed by a highly permeable sand columns was adopted and examined as a countermeasure to reduce the upward excess water pressure and improve the excavation bottom safety. The efficiency of this countermeasure has been tested and proven numerically.

More recently, Cheng et al. [34] discussed various methods used for the seepage failure problem analysis. Based on the use of various numerical methods and computer programs, the authors reported that the finite element method is the most adaptable method among all, while the analytical method is actually sufficient for normal engineering problems. The authors also collected several cases from different projects in Hong Kong, and stated that the importance of a good seepage failure analysis is well recognized by many engineers. Dang & Khabbaz [35] numerically investigated the stability against seepage failure by boiling of a sandy soil excavation supported by a sheet piled-cofferdam, using the FEM in 2D- and 3Dflow conditions. Their results demonstrated that the cofferdam stability significantly improved with an increase in the cofferdam size. Meanwhile, it was found that the shallow penetration depth of the sheet piles and the deeper excavation level within the cofferdam had a substantial influence on the excavation base stability when the cofferdam size effect was taken into account.

Koltuk & Fernandez-Steeger [36] performed a coupled hydro-mechanical analysis using the FEM in AXISflow conditions to examine seepage failure by heaving of pit excavation supported by a circular sheet pile wall constructed in homogeneous cohesionless soils. The FEM analysis results show relatively different failure zones compared to the failure plane of Terzaghi's method. However, the difference between the critical hydraulic head differences ΔH_c obtained from the FEM analysis $\Delta H_{c\ (FEM)}$ and Terzaghi's method $\Delta H_{c\ (Terzaghi)}$ is negligible. The maximum and minimum ratios of $\Delta H_{c\ (FEM)}$ to $\Delta H_{c\ (Terzaghi)}$, ($\Delta H_{c\ (FEM)}/\Delta H_{c\ (Terzaghi)}$), are respectively equal to 1.07 and 0.96.

In geotechnical engineering, different excavations types (long, short, wide and narrow) are encountered, and different cofferdams shapes (rectangular, square or circular) are used. Also, complex cases are generally approached using simplifying assumptions and adopting large safety factors to account for uncertainties. To this effect, if the excavation length is not large enough to consider it under 2D flow conditions, the real conditions and phenomena generated by the considered case must be appropriately taken into account in design to improve accuracy and safety. So, more accurate and appropriate approaches, using numerical simulations in 3D- or AXISflow conditions, are needed to analyse seepage failure problem, asses the H_c/D values, and predict seepage failure modes for such case.

Based on the review of previous methods presented above and with respect to investigations carried out to date, it should be noted that most previous research focuses solely on assessing flow rate, exit gradient and safety factors against seepage failure (or hydraulic failure). In addition, the radius variation effect on seepage failure modes and the H_c/D value have not been addressed in details for the circular cofferdam case. In AXISflow conditions, rigorous solutions do not appear to exist for the H_c/D values and the corresponding seepage failure modes predictions according to soil properties, interface characteristics and cofferdam radius.

The purpose of the present study is to take advantage of the numerical computation, which is able to deal with complex cases in their globality without any simplifying assumptions, and which does not require in advance the specification of the seepage failure shape needed for previous methods based on the prismatic failure concept, to analyse the stability against seepage failure of a soil surrounded by a circular cofferdam wall embedded in a single-layered

cohesionless homogeneous sand, and to study the effects of cofferdam radius, soil properties and soil-wall interface characteristics on the H_c/D values and seepage failure modes. The present results obtained from computation, using a numerical model of groundwater seepage flow in AXISflow conditions, are presented in tables and graphs, and compared with previously published results available in the literature [4, 6, 7, 12, 14, 15] in order to explain the sensitivity of the seepage failure modes and H_c/D critical values to soil properties, interface characteristics and cofferdam radius ratio R/D. Also, to describe and clarify the 3D seepage failure modes of soil within a cylindrical cofferdam. In the present study, dimensionless H/D and R/D ratios were used to allow the adaptability of the present results to different critical water levels, circular cofferdam sizes and embedment depths (various configurations). A flowchart of the research methodology employed in this study is shown in Figure 4.

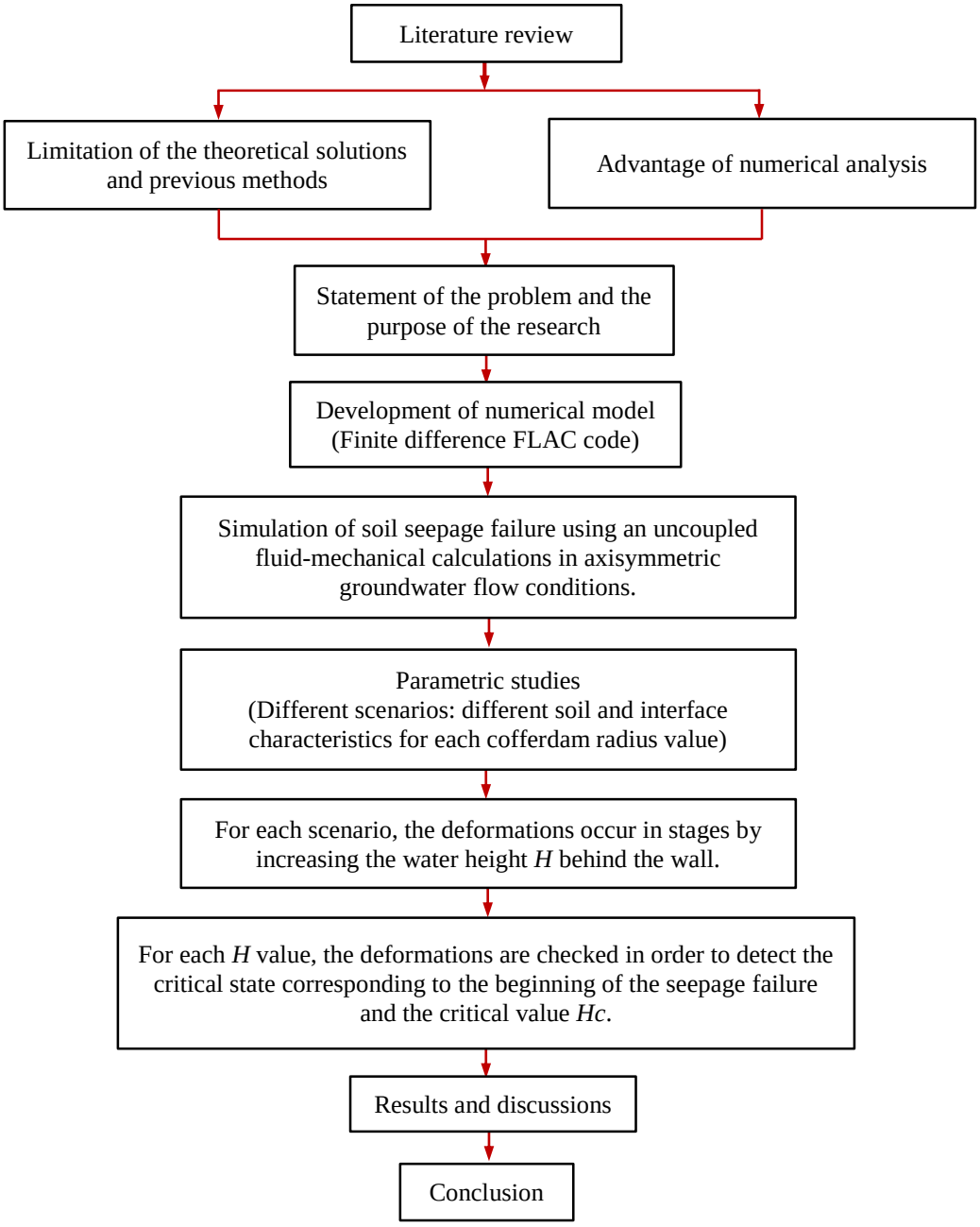

Figure 4. Research methodology flow chart

2. Problem Definition

This paper aims for the numerical analysis of seepage failure modes, in axisymmetric groundwater flow conditions, within a cylindrical cofferdam installed in a homogenous isotropic semi-infinite sandy soil. The circular wall with radius R is embedded at a depth D below the horizontal surface level of the subsoil, and it is subjected to hydraulic head difference H as shown in Figure 5. The water head H behind the circular wall is gradually increased until the occurrence of the soil seepage failure (critical state). The analysis is performed using the FLAC code based on the explicit finite

difference method. The continuous medium mechanical behaviour when it reaches equilibrium or plastic flow is calculated numerically by this code. The explicit Lagrangian calculation scheme and the mixed-discretization zoning technique [37] used in FLAC ensure that plastic failure and flow are very accurately modelled.

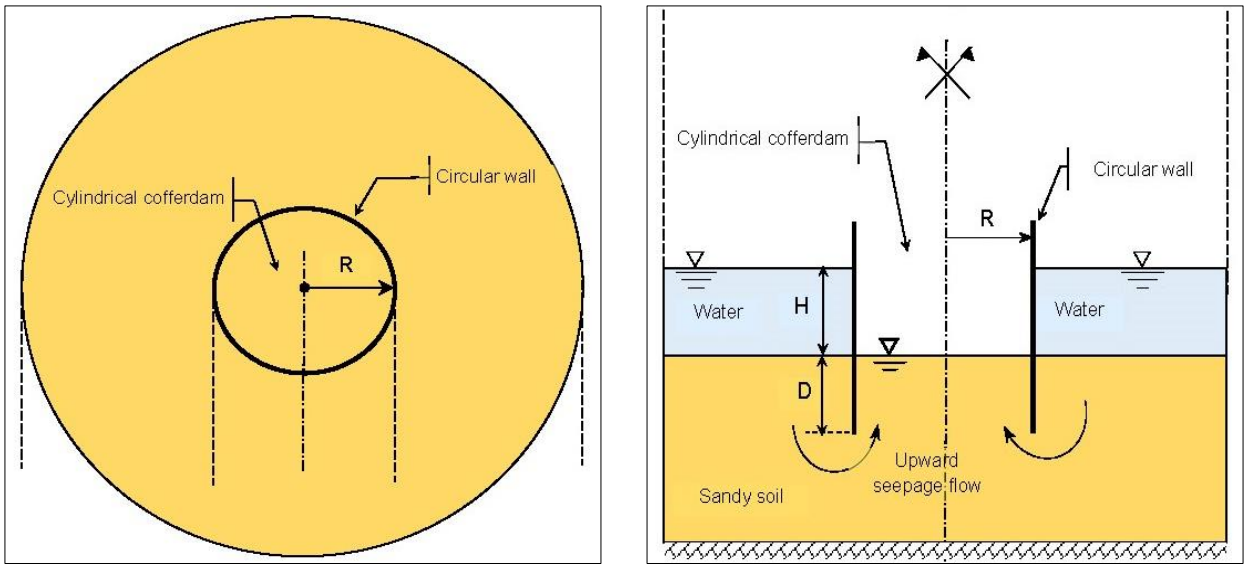

(a) (b)

Figure 5. Studied case: (a) Plan view; (b) Profile view: Schematic sketch of cylindrical cofferdam inducing axisymmetric flow conditions

The soil behaviour is modelled by using the elastic-perfectly plastic no-associative Mohr–Coulomb model encoded in FLAC. Depending on the dimensionless ratio *R/D* of the radius *R* to the penetration depth *D*, on soil properties and soil-wall interface characteristics, all subsequent results are given for a ratio of saturated soil density to water density $\gamma_{sat}/\gamma_w = 2$, a soil elastic bulk modulus $K = 30$ MPa and a soil shear modulus $G = 10$ MPa. To study how the H_c/D value and the seepage failure modes are affected by the cofferdam radius, ten radius ratios $R/D = 0.5$; 1; 1.5; 2; 3; 5; 10; 15; 20 and 30 are examined. For each radius ratio, five values of the internal soil friction angle $\varphi = 20°$; 25°; 30°; 35° and 40°, four values of the interface friction angle $\delta/\varphi = 0$; 1/3; 2/3 and 1, and three values of the soil dilatancy angle $\psi/\varphi = 0$; 1/2 and 1, are considered in this numerical analysis.

3. FLAC Numerical Simulation

For this problem, numerical analysis was performed in AXISflow conditions. Figure 6 shows a typical mesh and mechanical boundary conditions retained in this analysis. The mesh size is refined in the wall vicinity where deformations and flow gradients are concentrated. The mesh lateral boundary is located at six times D from the wall and the mesh depth is equal to five times D for every cofferdam radius to minimize boundary effects. For boundary conditions, it is assumed that the bottom boundary is fixed in both horizontal and vertical directions at that time the right and left lateral boundaries are fixed only in the horizontal direction.

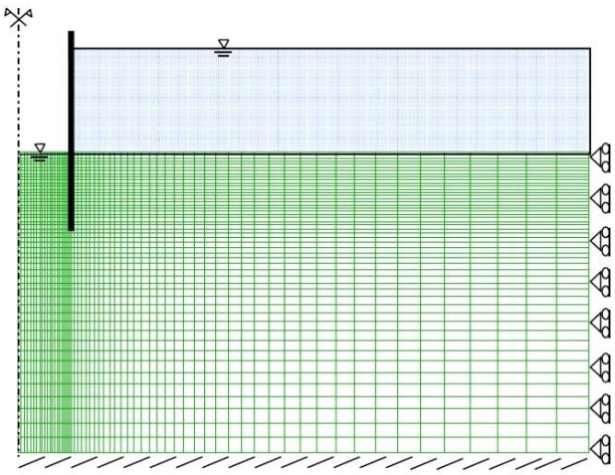

Figure 6. Mesh used and limit boundary conditions

For axisymmetric problem, structural elements combined in FLAC do not work. Therefore, the sheet pile wall is modelled by thin fixed impermeable membrane elements connected to the soil grid via interface elements attached on both sides. The interface model programmed in the FLAC code, whose components are shown in Figure 7, was used to simulate the soil-wall contact governed by the elastoplastic constitutive law based on the Mohr-Coulomb criterion. The logic contact for the interface sides is similar in nature to the interface used in the distinct element method [37]. The Coulomb shear-strength criterion is represented by the spring and the slider in the tangential direction (Figure 7). The spring in the normal direction and the limit strength represent the normal contact. The soil-wall interface has a friction angle δ, a cohesion c = zero kPa, a normal stiffness K_n = 10.E9 Pa/m, and a shear stiffness K_s = 10.E9 Pa/m. These values of K_n and K_s are selected to approximate the results for the case where the wall is rigidly attached to the soil grid.

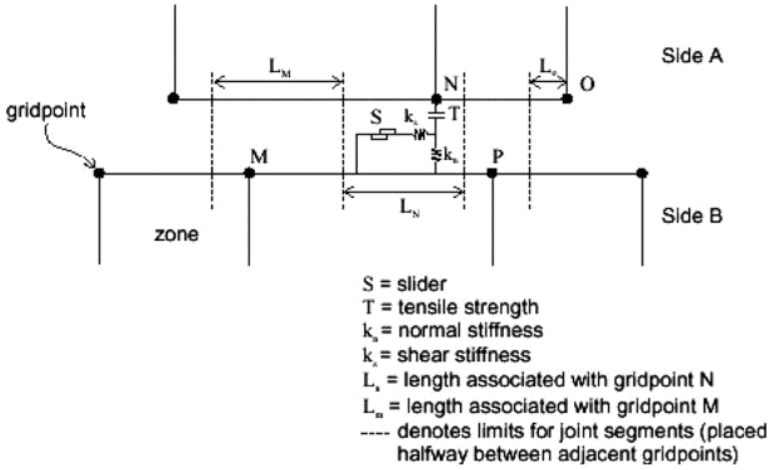

Figure 7. Interface element used [5]

The FLAC code has the ability to perform both flow-only and coupled fluid-mechanical analysis. Coupled analysis may be performed with any of the mechanical material models in FLAC. Several modelling strategies are available to approach the coupled processes. But a fully coupled quasi-static hydro-mechanical analysis with FLAC is often time-consuming and sometimes even unnecessary. There are numerous situations in which, some level of uncoupling can be performed in order to simplify the analysis and speed the calculation.

The present analysis is performed in effective stress using the groundwater configuration as an uncoupled hydro-mechanical calculations in AXISflow conditions. To identify the critical states corresponding to the onset soil seepage failure by heaving or boiling, the following three simulation procedure steps are adopted:

- Step 1: Initial state: At first, the geostatic stresses are computed assuming the material is elastic. The groundwater level is assumed to be located at the ground surface. The initial pore pressure and effective stresses are established using the fish library function assuming that the ratio of the effective horizontal stress to the effective vertical stress at rest K_0 is assumed equal to 0.5. At this stage, some stepping is required to carry the model to equilibrium. The reason is that an additional stiffness from interface elements produces an imbalance that necessitates some stepping to equilibrate the model.
- Step 2: Pore pressure distribution induced by hydraulic head loss H: The model is run in groundwater flow mode under hydraulic limit conditions. The calculation continues until the steady-state is reached.
- Step 3: Mechanical response: The model mechanical response is examined for the pore pressure distribution established in the previous step by cycling the model to equilibrium or failure in mechanical mode.

Steps 2 and 3 are repeated with progressive increase in the hydraulic head loss H until soil seepage failure occurs.

Numerical plotting of velocity vectors, displacement vectors and maximum shear strain rate distribution allows visualisation of the seepage failure mode (failure mode predictions). Therefore, for every cofferdam radius, H_c/D value is examined for various governing parameters: internal soil friction φ, soil dilatancy ψ and interface friction δ.

4. Results and Discussion

The results of the present study, for H_c/D values and seepage failure modes, are well structured and presented in tables and graphs depending to soil and interface characteristics for different values of the cofferdam radius ratios R/D. Then discussed and compared to the previous work solutions reported in the literature.

4.1. For large Values of Radius Ratios R/D ≥ 20 (Large Cofferdam)

First, numerical simulations are performed for large values of cofferdam radius ($R/D \geq 20$). The results show no effect of increasing radius ratios R/D more than 20. A comparison of the present results for R/D = 20 with those of previous work is discussed.

4.1.1. Comparison with Previous Work

For R/D = 20, the obtained results from computation in AXISflow conditions, listed in Table 1 of critical hydraulic head loss H_c/D, provide results very closely to computation results in 2Dflow conditions published by Benmebarek et al. [15]. Moreover, the same forms of seepage failure mechanisms, as those obtained by the authors [15], are observed according to the profile or plan view of downstream soil deformation. The results clearly indicate that the seepage failure of downstream soil in AXISflow conditions always corresponds to bulk heaving, except in the dilatant sand case (Dense sand) with ψ/φ >1/2, when $\varphi \geq 35°$ and with a perfectly rough interface δ/φ = 1 where failure by boiling would occur. It can be seen that seepage failure by boiling starts from a critical hydraulic head loss value H_c/D = 3.15. This value is very close to the theoretical value found by Terzaghi's method [6, 7] H_c/D = 3.14 corresponding to the case of exit hydraulic gradient attaining the critical hydraulic gradient value. The Figure 8 shows the seepage failure mode indicated by the displacement field and the corresponding distribution of maximum shear strain rates obtained in the case when φ = 40°, δ/φ = 1, ψ/φ = 1 and H_c/D = 3.15 where boiling phenomenon is observed in downstream soil on a part of the excavation base (Partial boiling-type failure). In addition, according to the plan view of the downstream soil deformation, for non-dilatant sand (loose sand) ψ/φ = zero, a heaving of a rectangular soil prism similar to that proposed by Terzaghi's method is obtained. The Figure 9 shows this type of seepage failure mode in the case when φ = 35°, ψ/φ = zero, δ/φ = 2/3 and H_c/D = 2.92 where bulk heaving of a rectangular soil prism is observed with a smaller width than the Terzaghi's method. However, for the dilatant sand $\psi/\varphi \geq 1/2$, a heaving of trapezoidal or pseudo-triangular soil prism is obtained as shown in Figure 10 for the case when φ= 35°, ψ/φ = 1/2, δ/φ = 2/3 and H_c/D = 2.97.

Table 1. Hc /D for different soil and interface parameters φ, δ/φ and ψ/φ when R/D=20 (large cofferdam)

δ/φ	ψ/φ	H_c/D				
		φ = 20°	φ = 25°	φ = 30°	φ = 35°	φ = 40°
0	0	2.63*	2.67*	2.74*	2.77**	2.80*
	1/2	2.64**	2.70**	2.79**	2.82**	2.89**
	1	2.64**	2.71**	2.81**	2.84**	2.92**
1/3	0	2.67*	2.78*	2.84*	2.90*	2.93*
	1/2	2.68**	2.82**	2.88**	2.94**	2.98**
	1	2.68**	2.84**	2.90**	2.96**	3.02**
2/3	0	2.72*	2.81*	2.89*	2.92*	2.96*
	1/2	2.73**	2.83**	2.92**	2.97**	3.11**
	1	2.73**	2.84**	2.93**	3.02**	3.15**
1	0	2.73*	2.84*	2.90*	2.94*	2.98*
	1/2	2.73**	2.87**	2.94**	3.02**	3.12**
	1	2.73**	2.89**	2.97**	3.04**	3.15***

Failure by heaving of rectangular (*) Trapezoidal or pseudo triangular (**) soil prisms, or by boiling (***).

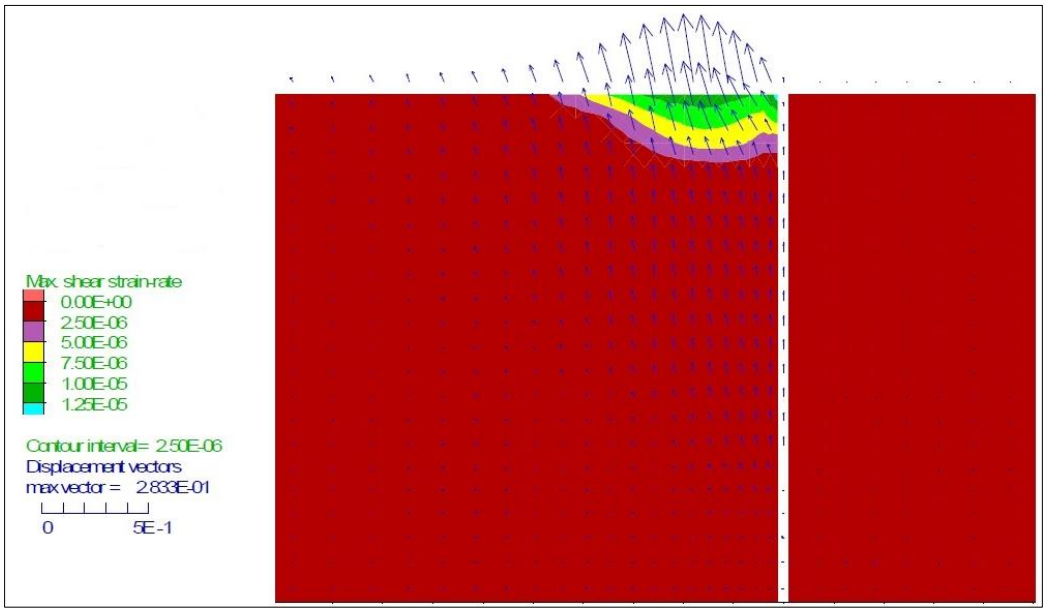

Figure 8. Displacement field and the corresponding distribution of maximum shear strain rates for R/D = 20, when φ=40°; ψ/φ=1; δ/φ=1 and H_c/D=3.15; Partial boiling type failure

On the other hand, by extending the plan view of these raised prisms (Figures 9 and10) in the third dimension around the cylindrical cofferdam axis (with a rotation angle θ = 360° around the revolution axis of the cylinder), we can imagine the top view of downstream soil upheaved surface, which will have the ring form with thickness equal to the prism width. According to this prism extension and from geometric evidence, these two failure types obtained (Figures 9 and10) correspond to the ring-type failure (Figure 3-a) observed and proposed by the method of Tanaka et al. [4] based on the prismatic failure concept in AXIS flow conditions.

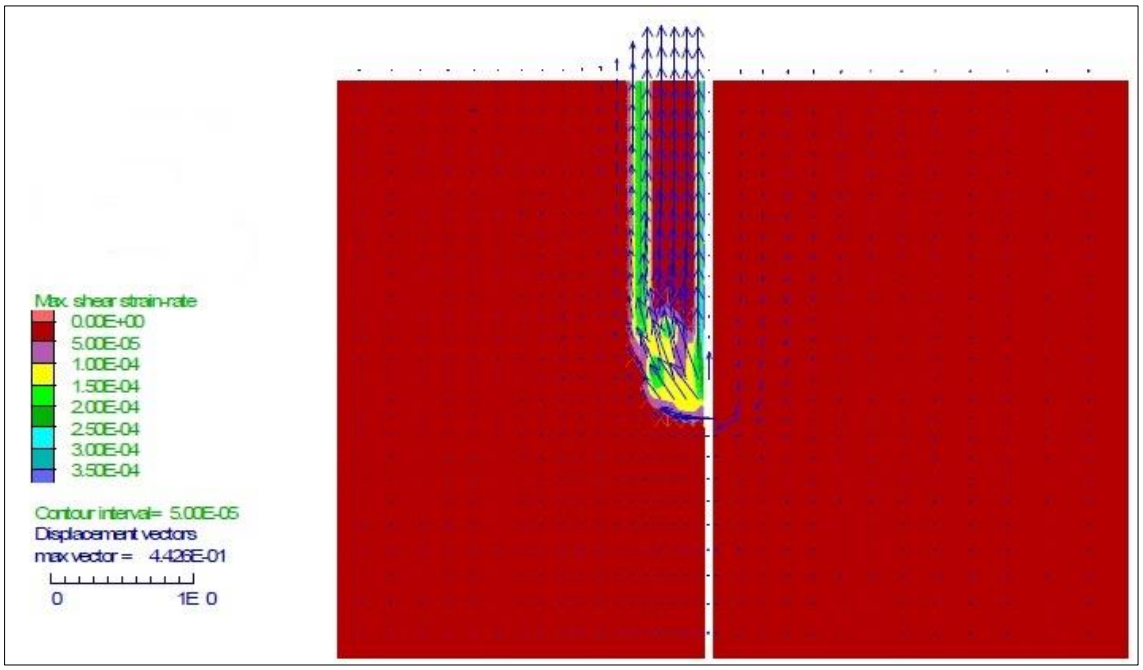

Figure 9. Displacement field and the corresponding distribution of maximum shear strain rates for R/D = 20, when φ=35°; ψ/φ=0; δ/φ=2/3 and H_c/D=2.92; Seepage failure by heaving of a rectangular prism

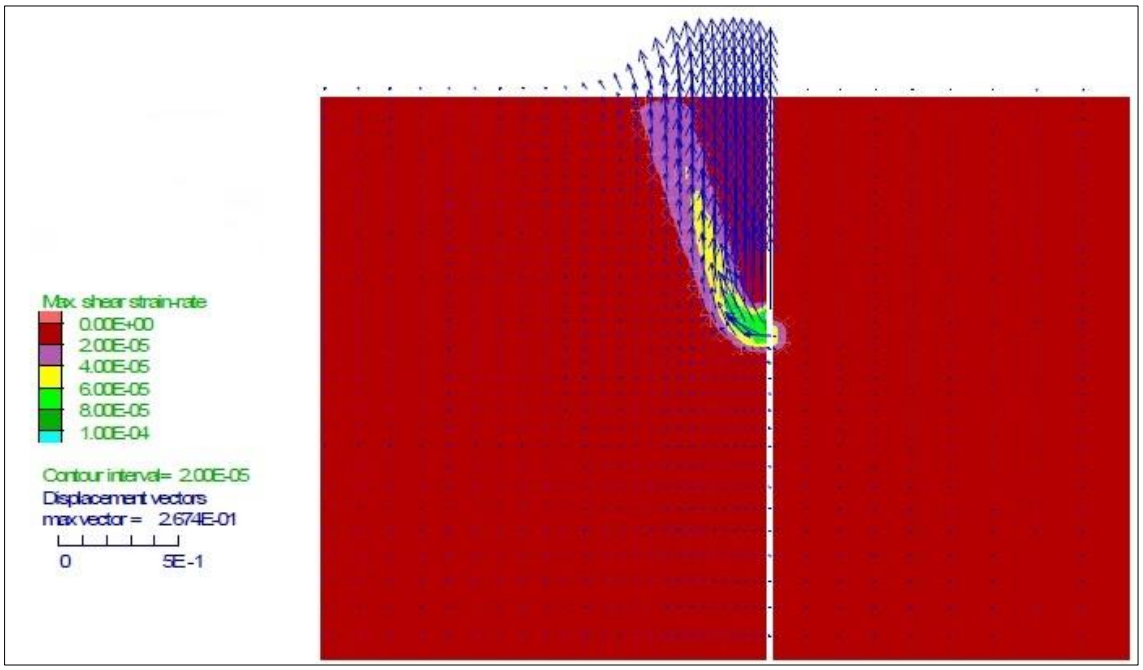

Figure 10. Displacement field and the corresponding distribution of maximum shear strain rates for R/D = 20, when φ=35°; ψ/φ=1/2; δ/φ=2/3 and H_c/D=2.97; Seepage failure by heaving of a trapezoidal (or pseudo-triangular) prism

4.1.2. Soil and Interface Characteristics Effects

The present simulation procedure indicates that soil dilatancy angle ψ has a significant effect on the seepage failure mode. This phenomenon can be explained as follows: when the downstream soil mass adjacent to the wall may expand

at failure, the shear forces induced on the prism sides block the rectangular prism heaving. Therefore, failure of a trapezoidal or pseudo-triangular prism appears instead. This corresponds to a kinematically admissible mechanism within the frame of limit analysis theory and Kastner [12] has experimentally observed this phenomenon. For large values of φ and ψ, shear forces on the wall embedment part and the horizontal soil expansion delay the trapezoidal (or pseudo-triangular) prism failure. Therefore, the surface exit gradient becomes critical before the bulk heaving of the trapezoidal (or pseudo-triangular) prism and initiates the boiling phenomenon.

From Table 1, for R/D = 20, δ/φ = zero, ψ/φ = 1 and φ varies from 20° to 40°, the critical value of H_c/D is in the range of 2.64 to 2.92. It is noted that for various values of φ Terzaghi's solution is H_c/D = 2.82, whereas that of Soubra et al. [14] solution is H_c/D = 2.78. Also, for φ = 40°, ψ/φ = 1 and δ/φ varies from zero to 1, the critical value of H_c/D is in the range of 2.92 to 3.15. Consequently, the present results show that the critical hydraulic head loss value H_c/D depends on the internal soil friction angle and the interface friction contrary to the results of Soubra & al. [14] and to those of Terzaghi's method [6, 7].

4.2. For Cofferdam Radius Ratios R/D < 20

4.2.1. Cofferdam Radius Ratios (R/D) effects

For radius ratios R/D < 20, the results show a significant sensibility of the critical hydraulic head loss value H_c/D to cofferdam radius ratios. Table 2 presents the computation results for R/D = 2. The H_c/D critical value is in the range of 1.75 to 2 and the same failure mechanisms are noted (Failure by heaving of rectangular (*), trapezoidal or pseudo-triangular (**) soil prisms, or by boiling (***)). The comparison of the present study results for R/D = 2 listed in Table 2 with results for R/D = 20 listed in Table 1 shows a decrease in H_c/D as well as in the sensibility to soil and interface characteristics.

Table 2. Hc /D for different soil and interface parameters φ, δ/φ and ψ/φ when R/D=2

δ/φ	ψ/φ	H_c/D				
		φ = 20°	φ = 25°	φ = 30°	φ = 35°	φ = 40°
0	0	1.75*	1.75*	1.76*	1.78*	1.80*
	1/2	1.75**	1.76**	1.80**	1.81**	1.83**
	1	1.75**	1.76**	1.81**	1.82**	1.85**
1 /3	0	1.76*	1.77*	1.79*	1.82*	1.84*
	1/2	1.77**	1.78**	1.81**	1.85**	1.88**
	1	1.77**	1.79**	1.83**	1.87**	1.90**
2/3	0	1.76*	1.78*	1.82*	1.86*	1.88*
	1/2	1.78**	1.79**	1.85**	1.89**	1.94**
	1	1.78**	1.80**	1.86**	1.91**	1.97**
1	0	1.77*	1.80*	1.84*	1.88*	1.91*
	1/2	1.79**	1.82**	1.87**	1.92**	1.98**
	1	1.80**	1.83**	1.88**	1.94**	2.00***

Failure by heaving of rectangular (*) or Trapezoidal or pseudo triangular (**) soil prisms, or by boiling (***).

To illustrate the radius effect, ten radius ratios R/D = 0.5; 1; 1.5; 2; 3; 5; 10; 15; 20 and 30 are numerically tested for two extreme cases of the present study as follows: Case 1 (Upper limit), characterized by φ=40°, ψ/φ=1 (Dilatancy) and δ/φ = 1 (Perfectly rough interface) and case 2 (Lower limit) characterized by φ=20°, ψ/φ=0 (No dilatancy) and δ/φ = 0 (Perfectly smooth interface). The present results plotted in Figure 11 clearly show the decrease in H_c/D with the decrease in R/D. This decrease is accentuated for lower value of R/D. For case 1: H_c/D decrease from 3.15 to 1.3, and for case 2: H_c/D decrease from 2.63 to 1.3. Then, the use of one soil column (2Dflow conditions) case overestimates the critical hydraulic head loss value. Moreover, it is clearly observed from Figure 11 that the sensibility to soil and interface characteristics decreases with the decrease in R/D and vanishes for small value of radius ratio $R/D \leq 0.5$.

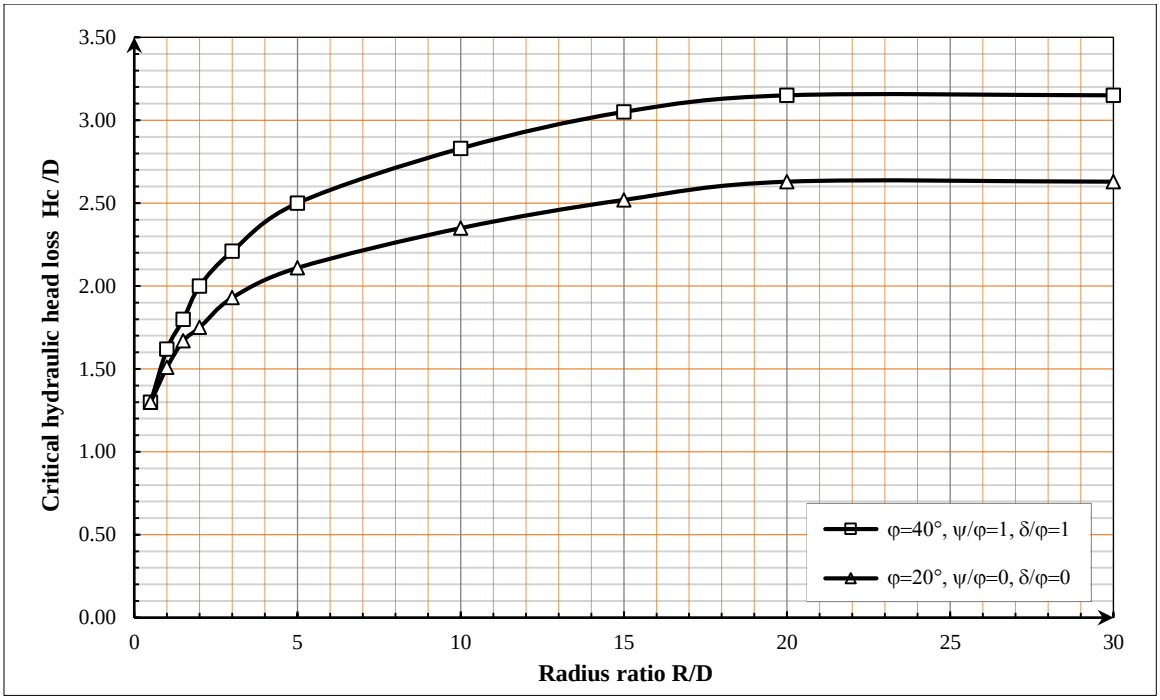

Figure 11. Decrease in Hc/D with the decrease in R/D: Hc/D vs R/D (Present results)

The present results also show that, for the small value case of R/D = 0.5, different seepage failure mechanisms depending on the soil and interface characteristics are obtained for the same value of H_c/D. On the one hand, for R/D = 0.5, Figure 12 shows the seepage failure mode in the case when φ = 35°, ψ/φ = 1 (Dense sand), δ/φ = 2/3 (rough interface), and H_c/D = 1.3, where the boiling phenomenon has propagated in the downstream soil of the entire excavation base (General boiling-type failure).

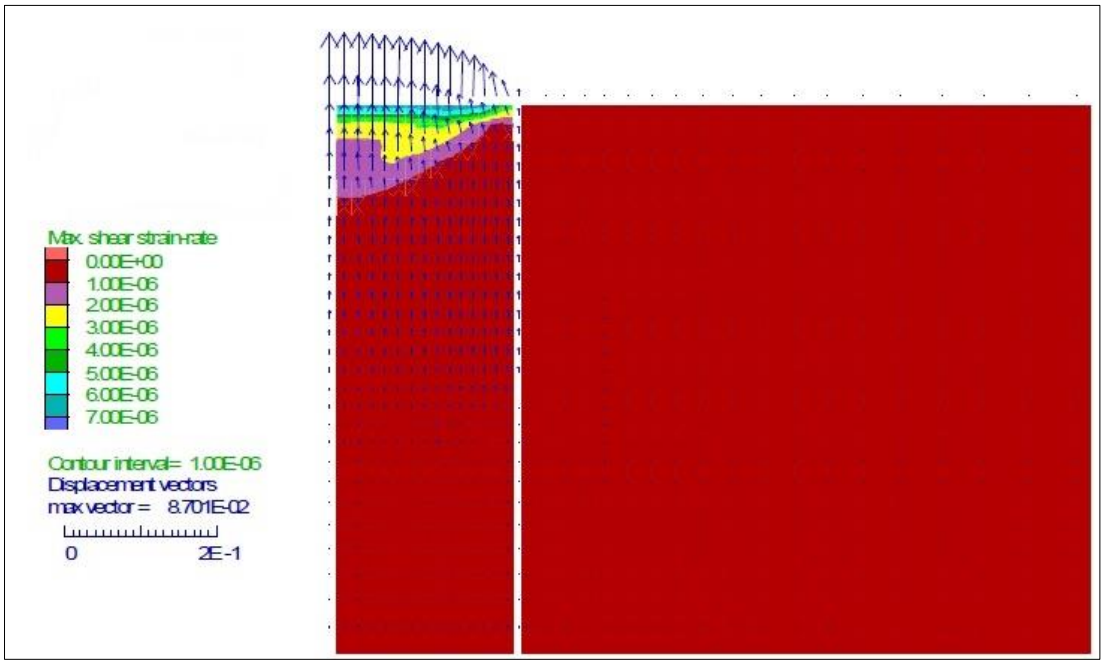

Figure 12. Displacement field and the corresponding distribution of maximum shear strain rates for R/D=0.5 when φ=35º; ψ/φ=1; δ/φ=2/3 and H_c/D=1.3; General boiling-type failure

On the other hand, for the same value R/D = 0.5, Figure 13 shows the seepage failure mode in the case when φ=35º, ψ/φ = 0 (Loose sand), δ/φ = 0 (perfectly smooth interface), and H_c/D = 1.3 where bulk heaving of a rectangular soil prism generalized in the entire downstream soil (Global heaving-type failure). These different modes of seepage failure are produced for the same value of H_c/D for which no sensibility to soil and interface characteristics is observed.

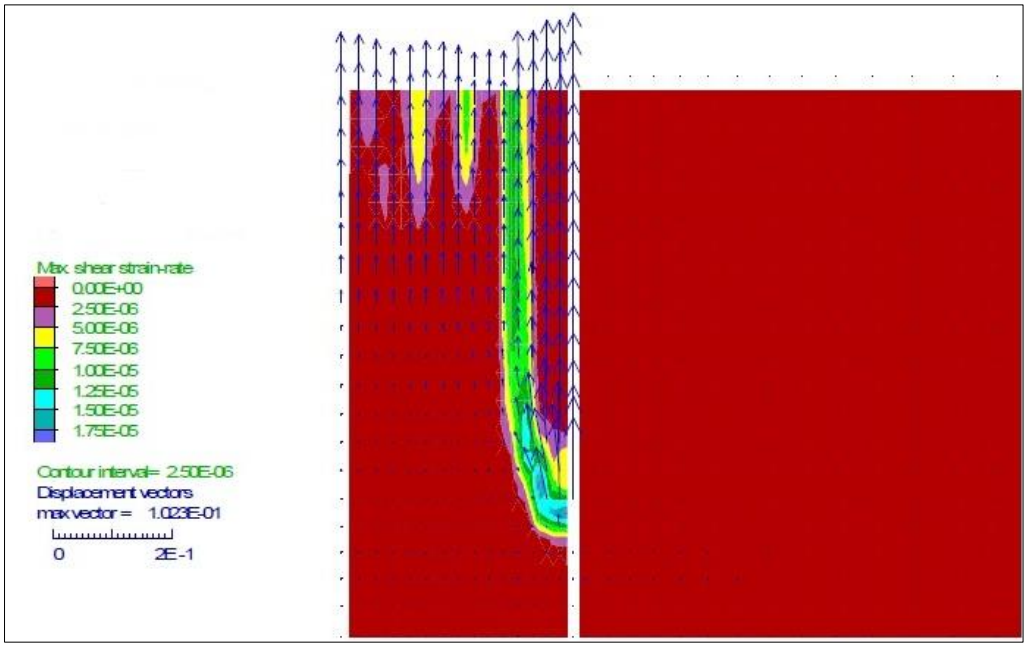

Figure 13. Displacement field and the corresponding distribution of maximum shear strain rates for R/D=0.5 when φ=35°; ψ/φ=0; δ/φ=0 and H_c/D=1.3; Global heaving-type failure

4.3. Descriptions of 3D Soil Seepage Failure Modes within a Cylindrical Cofferdam

Based on the present study results discussed above in various scenarios examined in AXISflow conditions, we try to explain more about seepage failure modes of downstream soil within cylindrical cofferdam, by providing graphic illustrations that show from geometric evidence the soil deformations in profile-, surface- and 3D-view (Figures 14 to 16), which allows us to make the following additional discussion and proposals.

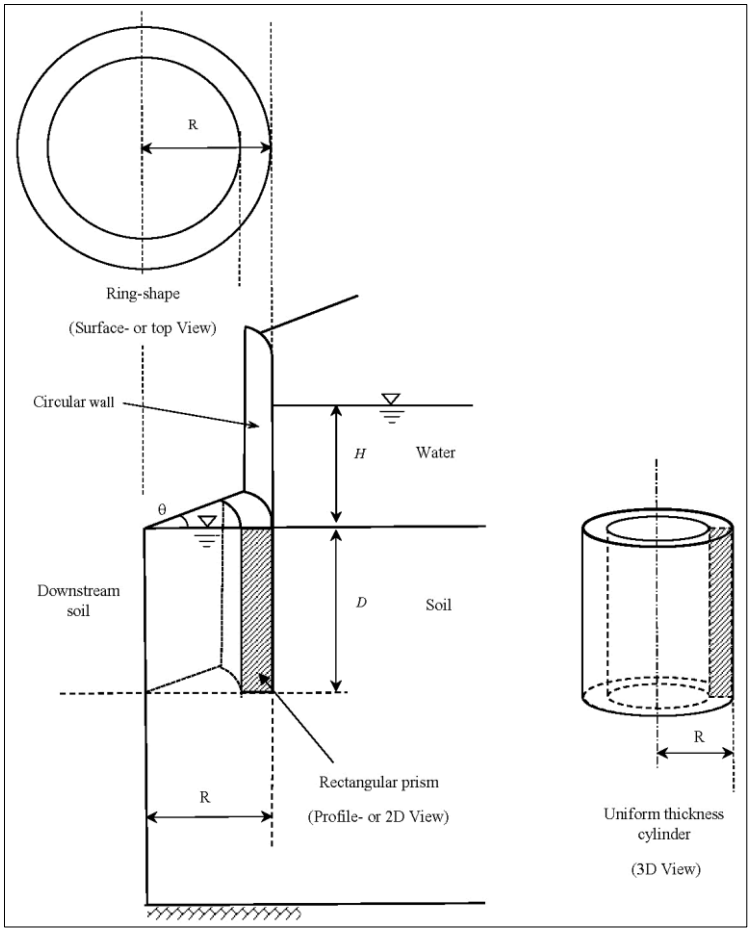

Figure 14. Uniform thickness cylinder-type failure for: R/D > 1, φ≥ 20°, δ/φ ≥ 0 and ψ/φ = 0 (No dilatancy)

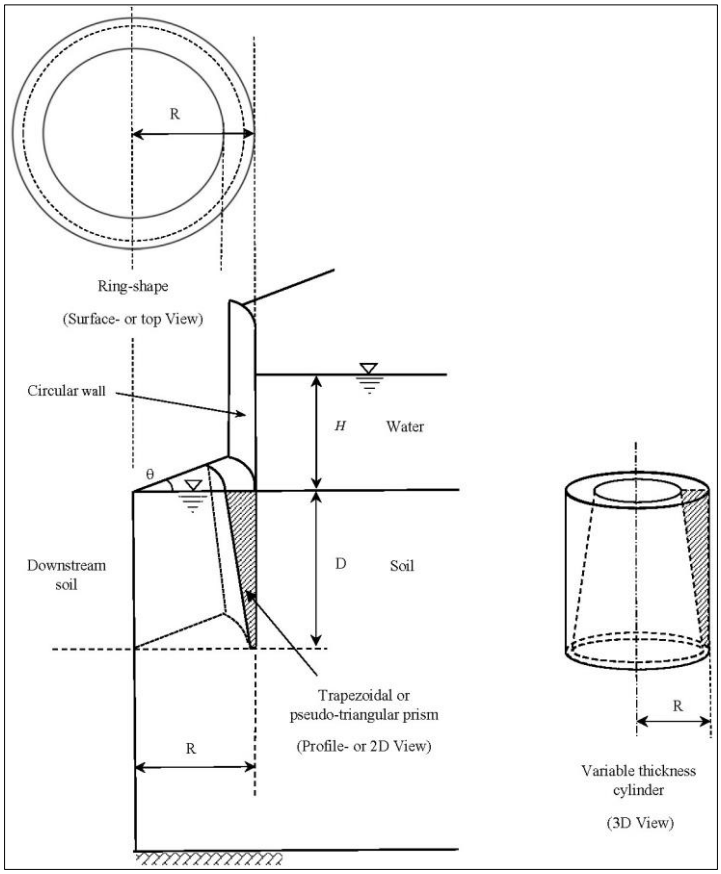

Figure 15. Variable thickness cylinder-type failure for: R/D > 1, φ≥ 20°, δ/φ ≥ 0 and ψ/φ ≥ 1/2 (Dilatancy). Except for the case when φ=40°, δ/φ = 1 and ψ/φ = 1

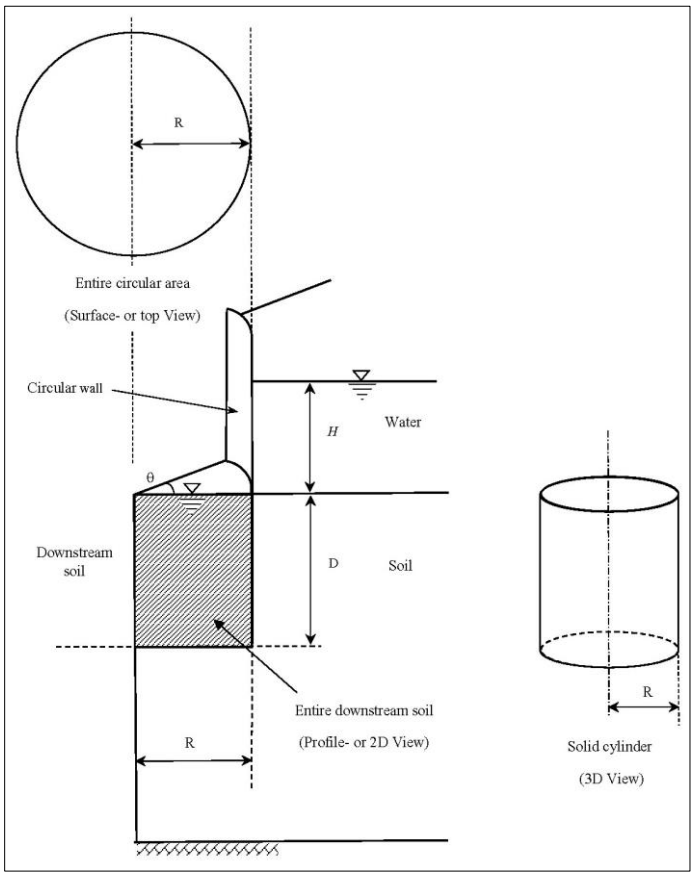

Figure 16. Solid cylinder-type failure for small value of R/D =0.5, when φ≥ 20°, ψ/φ ≥ 0 (No dilatancy), δ/φ = 0 (perfectly smooth interface)

Therefore, according to the surface deformation of downstream soil, we numerically obtained the same seepage failure types observed experimentally by Tanaka et al. (2000) [4], which they appropriately termed as "Ring-type failure" (Figure 3-a) for the case of seepage failure by heaving of prism (Figure 9 & 10) and "Punching failure" (Figure 3-b) for the case of general boiling-type failure (Figure 12). But according to the 3D view of the soil surrounded by the cylindrical cofferdam, the upheaved soil body has the shape of a cylinder, which can be solid (Figure 16), or hollow with a uniform or variable thickness (Figures 14 and 15). For the present case study, we suggest the following terms for the 3D shape of the seepage failure mode: "Uniform thickness cylinder-type failure" corresponding to the heaving of a rectangular prism (Figure 14); "Variable thickness cylinder-type failure" for the heaving of a trapezoidal or pseudo-triangular prism (Figure 15); and "Solid cylinder-type failure" for the global heaving of the entire downstream soil (Figure 16). For the boiling phenomena, we maintain the same terms: "partial boiling-type failure" and "global boiling-type failure" mentioned above. All this depends on the soil properties, the interface characteristics, and the cofferdam radius.

5. Conclusions

In this study, the soil seepage failure problem within a cylindrical cofferdam has been numerically analysed in axisymmetric groundwater flow conditions without any simplifying assumptions and without prior specifications of the failure mechanism scheme required for previous methods reported in the literature based on the prismatic failure concept. In addition, the effects of the cofferdam radius and various parameters of soil and interface are taken into account in this analysis. Numerical computations of the H_c/D critical values and seepage failure modes of homogenous cohesionless sandy soils within a cylindrical cofferdam have been performed using the FLAC code for various scenarios. The effects of the cofferdam radius ratio R/D, internal soil friction φ, soil dilatancy ψ and interface friction δ on the H_c/D value and seepage failure modes have been studied. The present results obtained in terms of the H_c/D critical values and their corresponding seepage failure modes (failure mode predictions) are presented in tables and graphs and compared to previously published results available in the literature. The sensitivity of seepage failure modes and H_c/D values to soil properties, interface characteristics, and cofferdam radius ratio R/D has been discussed and proven. Based on the 3D view of the downstream soil deformations, the 3D seepage failure modes of the soil within a cylindrical cofferdam have been described and the corresponding new terms have been proposed. In the present study, dimensionless H/D and R/D ratios were used to allow the present results to be adapted to different critical water levels, circular cofferdam sizes, and embedment depths (various configurations). And to provide decision support for practical design problems of circular cofferdams in the presence of water flow. A number of conclusions can be made from this study:

- For the large value of radius ratio R/D ≥ 20 (large cofferdam), according to the plan view of downstream soil deformation, the seepage failure mode in AXISflow conditions is the same as in 2Dflow conditions, where soil prism adjoining the wall upheaves (heaving-type failure). Except for the dilatant sand case (Dense sand), with $\psi/\varphi \geq 1/2$, when $\varphi \geq 35°$ and with a perfectly rough interface soil-wall $\delta/\varphi = 1$, where boiling-type failure occurs;
- For $R/D = 20$, the boiling-type failure starts from a critical hydraulic head loss value $H_c/D = 3.15$, which corresponds to a partial boiling-type failure, and it is very close to the theoretical value found by Terzaghi's method $H_c/D = 3.14$;
- For R/D varying from 20 to 0.5, the critical hydraulic head loss value H_c/D, corresponding to the onset of downstream soil seepage failure caused by upward seepage flow, decreases significantly with the decrease in R/D. For instance, when R/D decreases from 20 to 0.5 the H_c/D decreases from 3.15 to 1.3;
- For $R/D < 20$, the effects of soil and soil-wall interface characteristics decrease with the decrease in radius ratio R/D and vanish completely for small radius ratio values ($R/D < 0.5$);
- For R/D > 1, according to the plan view of downstream soil deformation, the seepage failure modes in AXISflow conditions are the same as those in 2Dflow conditions:
  - The boiling-type failure only appears for dense sand in which $\psi/\varphi > 2/3$ (Dilatancy), $\varphi \geq 35°$ and a perfectly rough soil-wall interface $\delta/\varphi = 1$. However, heaving-type failure occurs for the other cases;
  - For $R/D = 2$, the boiling-type failure starts from $H_c/D = 2.00$;
  - The present simulation procedure results show that soil dilatancy angle ψ has a significant effect on the seepage failure modes. For a dilatant sand, a failure by heaving of a trapezoidal or pseudo-triangular prism of soil is obtained. But for other cases (non-dilatant sand), a failure by heaving of a rectangular prism occurs. According to the 3D view of downstream soil deformation at failure, these two failure types corresponding to "Variable thickness cylinder-type failure" and "Uniform thickness cylinder-type failure" respectively;
  - The upheaved rectangular prism of downstream sand obtained has a width smaller than that resulting from Terzaghi's method.
- For the small value of radius ratio $R/D = 0.5$, different seepage failure mechanisms depending on the soil and soil-wall interface characteristics are obtained for the same value of $H_c/D = 1.3$:

- The case when φ= 35°, ψ/φ = 1 (Dense sand), δ/φ = 2/3 (Rough interface), where the boiling phenomenon has propagated in the entire excavation base soil (General boiling-type failure);
- The case when φ= 35°, ψ/φ = 0 (Loose sand), δ/φ = 0 (Perfectly smooth interface), where bulk heaving of a rectangular soil prism generalized in entire downstream soil (Global heaving-type failure), which corresponds to "Solid cylinder-type failure" according to the 3D view of downstream soil deformation.

6. Declarations

6.1. Author Contributions

Conceptualization, B.A., B.N. and B.S.; methodology, B.A.; writing—original draft preparation, B.A; writing—review and editing, B.A, B.N. and B.S. All authors have read and agreed to the published version of the manuscript.

6.2. Data Availability Statement

The data presented in this study are available in the article.

6.3. Funding

The authors received no financial support for the research, authorship, and/or publication of this article.

6.4. Acknowledgements

The authors express their gratitude to the Directorate General for Scientific Research and Technological Development of the Ministry of Higher Education and Scientific Research of Algeria.

6.5. Conflicts of Interest

The authors declare no conflict of interest.

7. References

[1] Tanaka, T., Hori, H., & Inoue, K. (2002). Boiling occurred within a braced cofferdam due to two-dimensionally concentrated seepage flow. International Symposium on Geotechnical Aspects of Underground Construction in Soft Ground, 23-25 October, 2002, Toulouse, France.

[2] Gui, M. W., & Han, K. K. (2009). An investigation on a failed double-wall cofferdam during construction. Engineering Failure Analysis, 16(1), 421–432. doi:10.1016/j.engfailanal.2008.06.004.

[3] Tanaka, T., Hirose, D., Kusaka, T., & Nagai, S. (2009). Characteristics of seepage failure of soil under various flow conditions. The 19th International Offshore and Polar Engineering Conference, 21-26 June, 2009, Osaka, Japan.

[4] Tanaka, T., Hayashi, K., & Yamada, M. (2000). Seepage failure of soil in an axisymmetric condition. GEOTECH-YEAR 2000 Developments in Geotechnical Engineering, 665-674, 27-30 November, 2000, Bangkok, Thailand.

[5] FLAC. (2016). Fast Lagrangian Analysis of Continua, ITASCA Consulting Group, Inc., Minneapolis, United States.

[6] Terzaghi, K. (1943). Theoretical Soil Mechanics. In Theoretical Soil Mechanics. John Wiley & Sons, Hoboken, United States. doi:10.1002/9780470172766.

[7] Terzaghi, K., & Peck, R. B. Soil Mechanics. Engineering Practice. John Wiley and Sons, Hoboken, Unites States.

[8] McNamee, J. (1949). Seepage into a sheeted excavation. Geotechnique, 1(4), 229–241. doi:10.1680/geot.1949.1.4.229.

[9] Marsland, A. (1953). Model experiments to study the influence of seepage on the stability of a sheeted excavation in sand. Geotechnique, 3(6), 223–241. doi:10.1680/geot.1953.3.6.223.

[10] Davidenkoff, R. (1956). To calculate the hydraulic heave. Wasserwirtschaft, 46(9), 230–235. (In German).

[11] Davidenkoff, R., & Franke, O. L. (1965). Investigation of the spatial seepage flow into a bunged excavation pit in open water. Tidewellenberechnung nach dem Universalprogramm der BAW, (22), 65-75. (In German).

[12] Kastner, R. (1982). Deep excavations in urban sites: Problems related to water proofing--sizing of braced supports. PhD Thesis, National Institute of Applied Sciences of Lyon, Lyon, France. (In French).

[13] Tanaka, T., & Verruijt, A. (1999). Seepage failure of sand behind sheet piles - The mechanism and practical approach to analyze. Soils and Foundations, 39(3), 27–35. doi:10.3208/sandf.39.3_27.

[14] Soubra, A. H., Kastner, R., & Benmansour, A. (1999). Passive earth pressures in the presence of hydraulic gradients. Geotechnique, 49(3), 319–330. doi:10.1680/geot.1999.49.3.319.

[15] Benmebarek, N., Benmebarek, S., & Kastner, R. (2005). Numerical studies of seepage failure of sand within a cofferdam. Computers and Geotechnics, 32(4), 264–273. doi:10.1016/j.compgeo.2005.03.001.

[16] Benmebarek, N., Bensmaine, A., Benmebarek, S., & Belounar, L. (2014). Critical Hydraulic Head Loss Inducing Failure of a Cofferdam Embedded in Horizontal Sandy Ground. Soil Mechanics and Foundation Engineering, 51(4), 173–180. doi:10.1007/s11204-014-9274-8.

[17] Pratama, I.T., Ou, CY. (2018). Analysis of Sand Boiling Failure in Deep Excavations. Proceedings of the 2nd International Symposium on Asia Urban GeoEngineering. Springer Series in Geomechanics and Geoengineering. Springer, Singapore. doi:10.1007/978-981-10-6632-0_10.

[18] Xiao, Q., & Wang, J. P. (2020). CFD-DEM simulations of seepage-induced erosion. Water (Switzerland), 12(3), 678. doi:10.3390/w12030678.

[19] Xiao, Q. (2020). Simulating the hydraulic heave phenomenon with multiphase fluid flows using CFD-DEM. Water (Switzerland), 12(4), 1077. doi:10.3390/W12041077.

[20] Benseghier, Z., Cuéllar, P., Luu, L. H., Bonelli, S., & Philippe, P. (2020). A parallel GPU-based computational framework for the micromechanical analysis of geotechnical and erosion problems. Computers and Geotechnics, 120, 103404. doi:10.1016/j.compgeo.2019.103404.

[21] Fukumoto, Y., Yang, H., Hosoyamada, T., & Ohtsuka, S. (2021). 2-D coupled fluid-particle numerical analysis of seepage failure of saturated granular soils around an embedded sheet pile with no macroscopic assumptions. Computers and Geotechnics, 136, 104234. doi:10.1016/j.compgeo.2021.104234.

[22] Wu, Y., Sun, Y., Zhang, X., Zhang, H., Ye, P., He, K., & Dong, C. (2022). Experiments and mechanisms for bottom vacuum leaching remediation of low permeability Cu, Zn-contaminated soil. Journal of Cleaner Production, 367, 133038. doi:10.1016/j.jclepro.2022.133038.

[23] Bouchelghoum, F. A. R. I. D., & Benmebarek, N. A. I. M. A. (2011). Critical hydraulic head loss assessment for a circular sheet pile wall under axisymmetric seepage conditions. Studia Geotechnica et Mechanica, 33(4), 3-23.

[24] Toumi, A., & Remini, B. (2021). Evaluation of Geology and Hydrogeology of the Water Leakage in Hammam-Grouz Dam, Algeria. Journal of Human, Earth, and Future, 2(3), 269–295. doi:10.28991/hef-2021-02-03-08.

[25] Tanaka, T., Toyokuni, E., & Ozaki, E. (1996). Prismatic failure-A new method of calculating stability against boiling of sand within a cofferdam. International Symposium on Geotechnical Aspects of Underground Construction in Soft Ground, 219-224, 15-17ril, 1996, London, United Kingdom.

[26] Tanaka, T., Tachimura, R., Kusumi, S., Nagai, S., & Inoue, K. (2016). Experimental findings of 3D seepage failure of soil within a cofferdam. Japanese Geotechnical Society Special Publication, 2(45), 1608–1613. doi:10.3208/jgssp.jpn-037.

[27] Fukumoto, Y., & Ohtsuka, S. (2018). 3-D direct numerical model for failure of non-cohesive granular soils with upward seepage flow. Computational Particle Mechanics, 5(4), 443–454. doi:10.1007/s40571-017-0180-5.

[28] Koltuk, S., Song, J., Iyisan, R., & Azzam, R. (2019). Seepage failure by heave in sheeted excavation pits constructed in stratified cohesionless soils. Frontiers of Structural and Civil Engineering, 13(6), 1415–1431. doi:10.1007/s11709-019-0565-z.

[29] Madanayaka, T. A., & Sivakugan, N. (2019). Simple solutions for square and rectangular cofferdam seepage problems. Canadian Geotechnical Journal, 56(5), 730–745. doi:10.1139/cgj-2018-0295.

[30] Becker, D. E., & Moore, I. D. (2006). Canadian manual of foundation engineering (4th Ed.). Canadian Geotechnical Society, Calgary, Canada.

[31] Madanayaka, T. A., & Sivakugan, N. (2020). Validity of the Method of Fragments for Seepage Analysis in Circular Cofferdams. Geotechnical and Geological Engineering, 38(2), 1547–1565. doi:10.1007/s10706-019-01111-9.

[32] Zhao, G. Qing, Yang, Y. You, & Meng, S. Yun. (2020). Failure of circular shaft subjected to hydraulic uplift: Field and numerical investigation. Journal of Central South University, 27(1), 256–266. doi:10.1007/s11771-020-4293-2.

[33] Ouzaid, I., Benmebarek, N., & Benmebarek, S. (2020). FEM optimisation of seepage control system used for base stability of excavation. Civil Engineering Journal, 6(9), 1739–1751. doi:10.28991/cej-2020-03091579.

[34] Cheng, Y. M., Chen, F., Zhu, Z., Yuan, C., & Li, L. (2021). Seepage Analysis for Construction, with Applications to Some Projects in Hong Kong. Geofluids, 2021. doi:10.1155/2021/6623816.

[35] Dang, L., Khabbaz, H. (2022). Numerical Investigation on the Boiling Stability of Sheet Piles Supported Excavations in Cohesionless Soil. CIGOS 2021, Emerging Technologies and Applications for Green Infrastructure. Lecture Notes in Civil Engineering, 203. Springer, Singapore. doi:10.1007/978-981-16-7160-9_40.

[36] Koltuk, S., & Fernandez-Steeger, T. (2022). Evaluation of seepage failure by heave in homogeneous cohesionless soils using finite element method. International Journal of Geotechnical Engineering, 1–10. doi:10.1080/19386362.2022.2042965.

[37] Cundall, P. A., & Hart, R. D. (1992). Numerical modelling of discontinue. Engineering Computations, 9(2), 101–113. doi:10.1108/eb023851.